

Close-Range Mainlobe Interference Suppression in FDA Radar

Yisheng Yan, Jie Cheng, Xingyi Meng, Wen-Qin Wang, *Senior Member, IEEE*, Chaogang Li

Abstract—Although phased-array (PA) radar can suppress sidelobe interference signals due to its directional beamforming capability, it cannot effectively suppress mainlobe interference signals located near the desired target. To address this limitation, we leverage the range-angle dependence of frequency diverse array (FDA) radar to mitigate close-range mainlobe interference. Unlike traditional adaptive beamforming methods, the proposed approach exploits the phase difference between interference and target signals induced by the frequency offset of FDA radar, enabling direct suppression of unwanted signals. The effectiveness of this method is validated through theoretical analysis and numerical simulations.

Index Terms—frequency diverse array (FDA) radar, mainlobe interference suppression, adjacent range bin, interference reconstruction.

I. INTRODUCTION

PA radar can effectively suppress sidelobe interference using traditional adaptive beamforming techniques, such as sidelobe blanking [1], sidelobe cancellation [2], and adaptive sidelobe nulling [3], or intelligent algorithms like feedback-induced coloration effects [4] and deep learning-based non-orthogonal multiple access [5]. However, these methods struggle to mitigate mainlobe interference, particularly close-range mainlobe signals [6], due to their overlapping angular and spectral characteristics with the desired target.

In contrast to PA radar, FDA radar can suppress close-range mainlobe interference signals. By employing a frequency offset Δf across its array elements, FDA generates a transmit beampattern dependent on angle, range, and time [7]. This unique property provides FDA with inherent advantages in the range domain, including additional degrees-of-freedom (DOFs) that enable targeted suppression of close-range interference within the mainlobe. Prior studies have explored frequency diverse

array multiple-input multiple-output (FDA-MIMO) radar for interference suppression. For instance, Xu et al. [8] cancelled deceptive interference using FDA-MIMO adaptive beamforming, while Lan et al. [10] and Yang et al. [11] achieved mainlobe deceptive interference suppression via broadened nulling beamforming and covariance matrix reconstruction, respectively. However, these methods depend on MIMO waveform diversity, a feature hindered by practical implementation challenges such as hardware complexity and signal orthogonal constraints.

In this letter, we propose a simpler algorithm to suppress mainlobe interference signals within 1 ~ 3 range resolution cells of the desired target. To our knowledge, this specific challenge—close-range mainlobe interference suppression without relying on waveform diversity constraints—has not been addressed in prior research. Furthermore, the proposed method requires only FDA radar and avoids the complexity of FDA-MIMO systems [10], [11], enabling straightforward implementation in practice.

This paper is organized as follows. Section II formulates the problem of close-range mainlobe interference suppression. Section III proposes the FDA-based suppression technique and details its operational principles and advantages. Section IV validates the method's efficacy and effectiveness through numerical simulations. Finally, Section V summarizes the key contributions and discusses their practical implications for radar system design.

II. PROBLEM FORMULATION

Consider the FDA radar with M -element transmit array and N -element receive array, where d_T and d_R denote respectively the inner-element spacing of transmit and receive array. The carrier frequency of the m th transmit element is expressed as

$$f_m = f_c + \Delta f_m, m = 0, 1, \dots, M - 1 \quad (1)$$

where Δf_m stands for the m th frequency increment to the reference carrier f_c . Let $s_m(t) = w_m s(t)$ be the baseband signal transmitted by the m th element, where $s(t)$ and w_m denote the waveform and transmit weight, respectively.

The m th transmitted signal can then be expressed as

$$s_m(t) \exp(j2\pi f_m t), 0 \leq t \leq T_s. \quad (2)$$

where T_s denotes the pulse duration. Assumed that, $\int_0^{T_s} s(t) s^*(t) dt = 1$, where $*$ is the conjugate operator.

Suppose there is a far-field target located at (θ_s, r_s) , the m th signal received by the n th receiving antenna element is

$$y_{n,m}(t; r_s, \theta_s) = \xi_{n,m}(t; r_s, \theta_s) s_m(t - \tau_{n,m}(t; r_s, \theta_s)) \cdot e^{j2\pi f_m(t - \tau_{n,m}(t; r_s, \theta_s))} \quad (3)$$

Manuscript received November 26, 2024; revised April 20, 2025.

This work is supported by National Natural Science Foundation of China under grant 61571081.

Y.S. Yan is a postdoctoral researcher of the School of Information and Communication Engineering, University of Electronic Science and Technology of China, Chengdu, P. R. China (e-mail: yishengyan0308@gmail.com).

J. Cheng is a doctoral graduate of the School of Information and Communication Engineering, University of Electronic Science and Technology of China, Chengdu, P. R. China (e-mail: chengjie@std.uestc.edu.cn).

Xingyi Meng is a technical staff at Xi'an Construction Engineering Fire Safety Technology Service Center, Xi'an 710002, P. R. China (e-mail: 771998934@qq.com).

W.-Q. Wang is a professor of the School of Information and Communication Engineering, University of Electronic Science and Technology of China, Chengdu, P. R. China (e-mail: wqwang@uestc.edu.cn).

C.G. Li is a research fellow of the Sichuan Institute of Aerospace Electronic Equipment, Chengdu, P. R. China (e-mail: 504977554@qq.com).

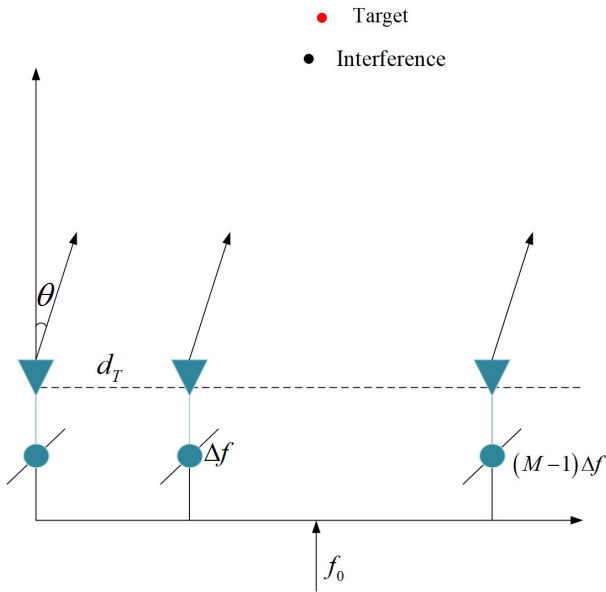


Fig. 1. ULA FDA configuration.

where $\xi_{n,m}(t; r_s, \theta_s)$ represents the reflection coefficient of the nm th corresponding path, and $\tau_{n,m}(t; r_s, \theta_s)$ is the corresponding propagation delay.

To simplify (3), we ignore the signal fluctuation in fast time and loss of generality. We then have

$$\xi_{n,m}(t; r_s, \theta_s) \approx \xi_s \quad (4)$$

$$\tau_{n,m}(t; r_s, \theta_s) \approx \tau_s + \tau_{T,m}(\theta) + \tau_{R,n}(\theta) \quad (5)$$

where $\tau_s = \frac{2r_s}{c}$, $\tau_{T,m}(\theta) = md_T \sin \theta / c$ and $\tau_{R,n}(\theta) = nd_R \sin \theta / c$. $\tau_{T,m}(\theta)$ and $\tau_{R,n}(\theta)$ being the corresponding propagation delays for transmitter and receiver, respectively. τ_s is the round-trip delay from the target to the radar phase center and c is the speed of light. In this case, the n th element received signal can be expressed as

$$\begin{aligned} y_n(t; r_s, \theta_s) &= \sum_{m=0}^{M-1} y_{n,m}(t; r_s, \theta_s) \\ &= \xi_s \sum_{m=0}^{M-1} s_m(t - \tau_s(r_s)) e^{j2\pi f_m t} \\ &\quad \cdot e^{j2\pi(f_m \tau_s(r_s) - f_c \tau_{T,m}(\theta_s) - f_c \tau_{R,n}(\theta_s))} \end{aligned} \quad (6)$$

It can also be rewritten in a vector formulation:

$$\mathbf{y}(t) = \xi_s \mathbf{a}(t; \theta_s, r_s) \mathbf{s}(t - \tau_s) \quad (7)$$

where

$$\mathbf{a}(\theta, r, t) = \mathbf{a}_R(\theta) \mathbf{a}_T^T(t, \theta, r) \quad (8)$$

$$\mathbf{a}_R(\theta) = \begin{bmatrix} 1 & e^{j2\pi \frac{d_R}{\lambda_c} \sin \theta} & \dots & e^{j2\pi \frac{d_R}{\lambda_c} (N-1) \sin \theta} \end{bmatrix}^T \quad (9)$$

$$\mathbf{a}_T(\theta, r, t) = \begin{bmatrix} e^{j2\pi f_1 t} & \dots & e^{j2\pi \frac{d_T}{\lambda_c} (M-1) \sin \theta} e^{j2\pi f_M t} \end{bmatrix}^T \quad (10)$$

$$\mathbf{s}(t) = [w_{T,0}s(t) \quad w_{T,1}s(t) \quad \dots \quad w_{T,M-1}s(t)]^T \quad (11)$$

with \mathbf{T} being the transpose operator and $\lambda_c = c/f_c$.

Consider multiple interference are located at (θ_{pj}, r_{pj}) , $p = 1, 2, \dots, P-1$, the overall received signals can be

represented by

$$\begin{aligned} \mathbf{y}(t) &= \xi_s \mathbf{a}(\theta_s, r_s, t) \mathbf{s}(t - \tau_s) \\ &+ \sum_{p=1}^{P-1} \varsigma_p \mathbf{a}(\theta_{pj}, r_{pj}, t) \mathbf{s}(t - \tau_{pj}) + \mathbf{n} \end{aligned} \quad (12)$$

where ς_p is the corresponding complex reflection coefficient, \mathbf{n} denotes zero-mean Gaussian noise, assumed to be white in space and time.

III. CLOSE-RANGE MAINLOBE INTERFERENCE SUPPRESSION

Based on the number of potential targets and interferences, we dynamically select distinct time slots within the one-pulse duration of a single receiving channel.

$$\begin{aligned} y(t_1) &= \xi_s \mathbf{a}(\theta_s, r_s, t_1) \mathbf{s}(t_1 - \tau_s) \\ &+ \sum_{p=1}^{P-1} \varsigma_p \mathbf{a}(\theta_{pj}, r_{pj}, t_1) \mathbf{s}(t_1 - \tau_{pj}) + n_1 \\ y(t_2) &= \xi_s \mathbf{a}(\theta_s, r_s, t_2) \mathbf{s}(t_2 - \tau_s) \\ &+ \sum_{p=1}^{P-1} \varsigma_p \mathbf{a}(\theta_{pj}, r_{pj}, t_2) \mathbf{s}(t_2 - \tau_{pj}) + n_2 \\ &\vdots \\ y(t_P) &= \xi_s \mathbf{a}(\theta_s, r_s, t_P) \mathbf{s}(t_P - \tau_s) \\ &+ \sum_{p=1}^{P-1} \varsigma_p \mathbf{a}(\theta_{pj}, r_{pj}, t_P) \mathbf{s}(t_P - \tau_{pj}) + n_P \end{aligned} \quad (13)$$

It can be rewritten as

$$\mathbf{Y} = \mathbf{A}\sigma + \gamma \quad (14)$$

where

$$\mathbf{Y} = [y(t_1) \quad y(t_2) \quad \dots \quad y(t_P)]^T \quad (15)$$

$$\mathbf{A} = \begin{bmatrix} \mathbf{v}(\theta_s, r_s, t_1) & \dots & \mathbf{v}(\theta_{(P-1)j}, r_{(P-1)j}, t_1) \\ \vdots & \ddots & \vdots \\ \mathbf{v}(\theta_s, r_s, t_P) & \dots & \mathbf{v}(\theta_{(P-1)j}, r_{(P-1)j}, t_P) \end{bmatrix} \quad (16)$$

$$\sigma = [\xi \quad \varsigma_1 \quad \dots \quad \varsigma_{P-1}]^T \quad (17)$$

$$\gamma = [n_1 \quad n_2 \quad \dots \quad n_P]^T \quad (18)$$

with $\mathbf{v}(\theta_p, r_p, t_j) = \mathbf{a}(\theta_p, r_p, t_j) \mathbf{s}(t_j - \tau_s)$.

The target and interference amplitude can be estimated as

$$\sigma_e = \mathbf{A}^{-1}(\mathbf{Y} - \gamma) \quad (19)$$

The interference information can be reconstructed and subtracted from the acquired original data to yield

$$\mathbf{g}(t) = \mathbf{y}(t) - \sum_{p=1}^{P-1} \varsigma_{ep} \mathbf{a}(\theta_{pj}, r_{pj}, t) \mathbf{s}(t - \tau_{pj}) \quad (20)$$

Accordingly, the received signal after interference suppression can then be formulated as

$$\mathbf{g}(t) = \mathbf{y}(t) - \mathbf{h}\varsigma_e \quad (21)$$

where

$$\mathbf{h} = \begin{bmatrix} \mathbf{a}(\theta_{1j}, r_{1j}, t) \mathbf{s}(t - \tau_{1j}) \\ \vdots \\ \mathbf{a}(\theta_{(P-1)j}, r_{(P-1)j}, t) \mathbf{s}(t - \tau_{(P-1)j}) \end{bmatrix}^T \quad (22)$$

$$\varsigma_e = [\varsigma_{e1} \quad \dots \quad \varsigma_{e(P-1)}]^T \quad (23)$$

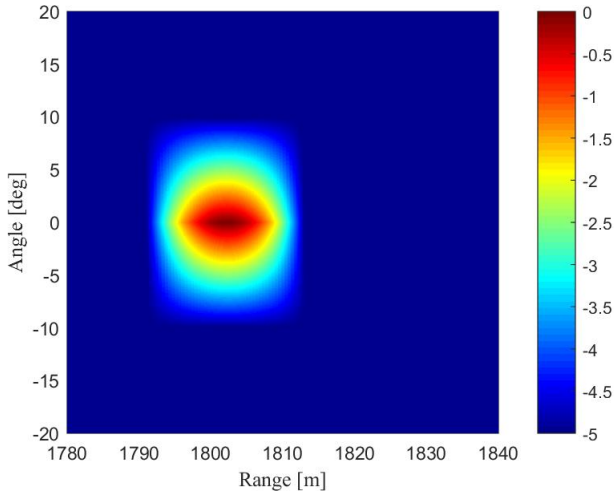


Fig. 2. Target and interference exist together with $ISR = -10\text{dB}$.

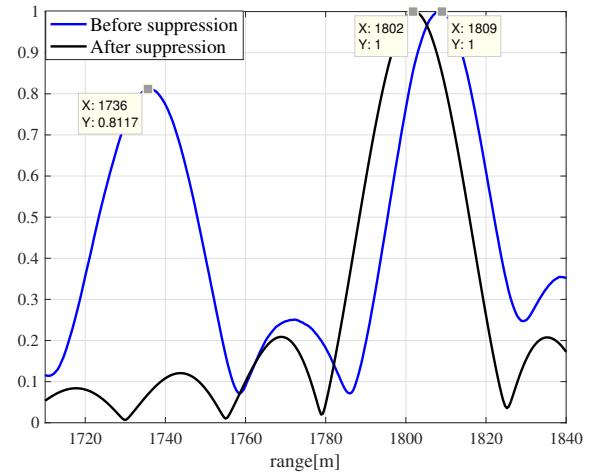


Fig. 4. Pulse compression results of target and interference with $ISR = -10\text{dB}$.

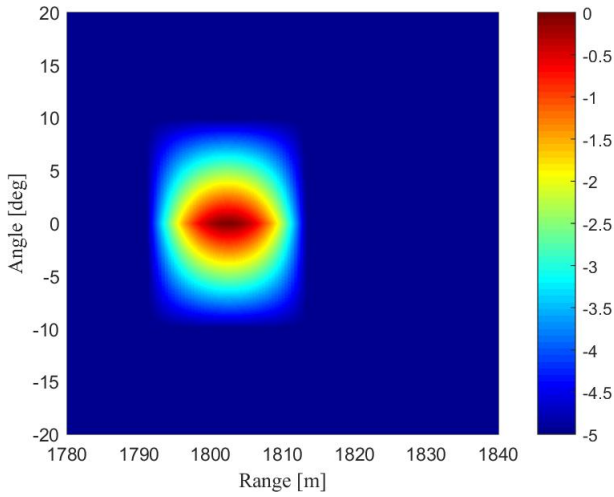


Fig. 3. The interference is suppressed by the proposed algorithm with $ISR = -10\text{dB}$.

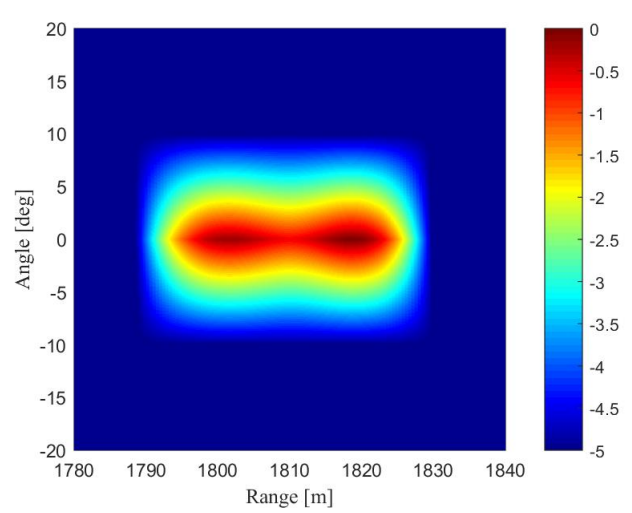


Fig. 5. Target and interference exist together with $ISR = 0\text{dB}$.

IV. NUMERICAL RESULTS

In this section, we validate the proposed interference suppression algorithm using numerical simulations, focusing on scenarios where the target and interference are in close-range proximity. Unless otherwise specified, the simulation parameters employed in the following examples are defined as follows. The reference frequency is $f_0 = 10\text{GHz}$, and the number of receiver and transmitter elements are $N = M = 8$, where the inter-element spacing are $d_T = d_R = \lambda_c/2$. The target of interest and the mainlobe interference are located at $(\theta_s, r_s) = (0^\circ, 1800\text{m})$ and $(\theta_j, r_j) = (0^\circ, 1818\text{m})$, respectively. The m th transmitted signal can then be expressed as $s_m(t) = \text{rect}\left(\frac{t}{T_p}\right) \exp(j\pi Kt^2)$, $0 \leq t \leq T_p, \forall m$, with $T_p = 5\mu\text{s}$ and bandwidth $B_p = 10\text{MHz}$. And K is the linearly modulated frequency, where $K = B_p/T_p$.

Mainlobe interference is well-documented to severely compromise target signal integrity. This degradation is governed by the correlation between the complex scattering coefficient of target and that of the interference, which is conventionally quantified by the interference-to-signal ratio

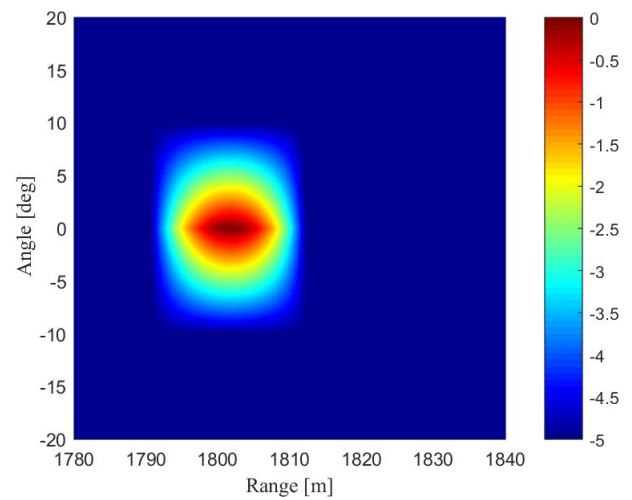


Fig. 6. The interference is suppressed by the proposed algorithm with $ISR = 0\text{dB}$.

(ISR). The original power spectra of the target and interference under varying ISR conditions are illustrated in

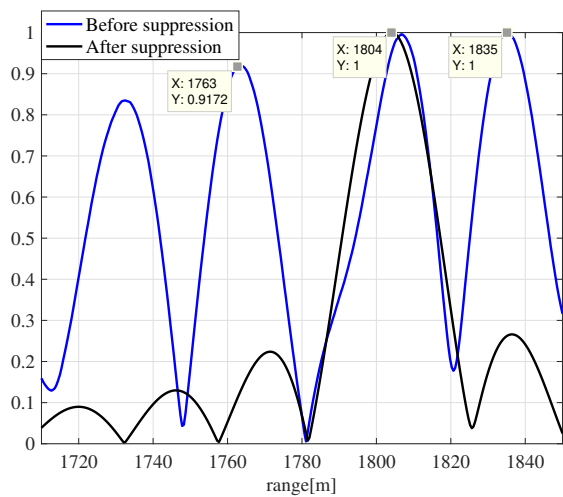


Fig. 7. Pulse compression results of target and interference with $ISR = 0dB$.

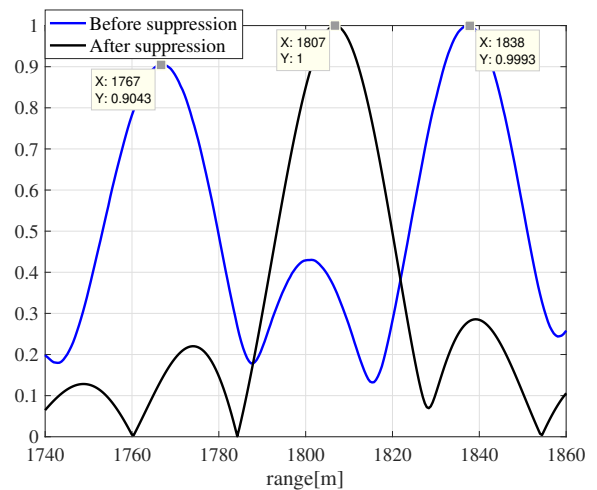


Fig. 10. Pulse compression results of target and interference with $ISR = 10dB$.

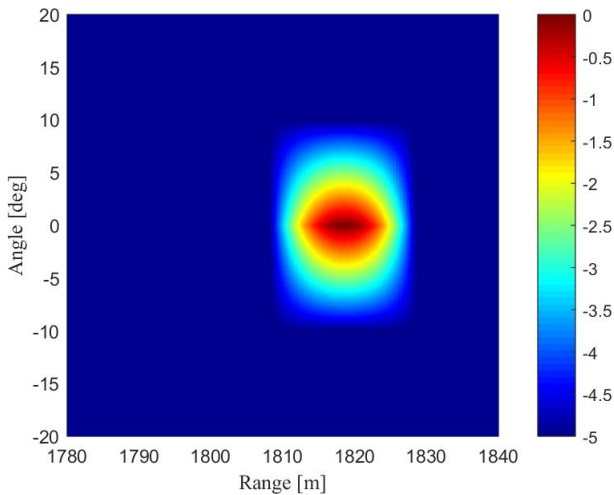


Fig. 8. Target and interference exist together with $ISR = 10dB$.

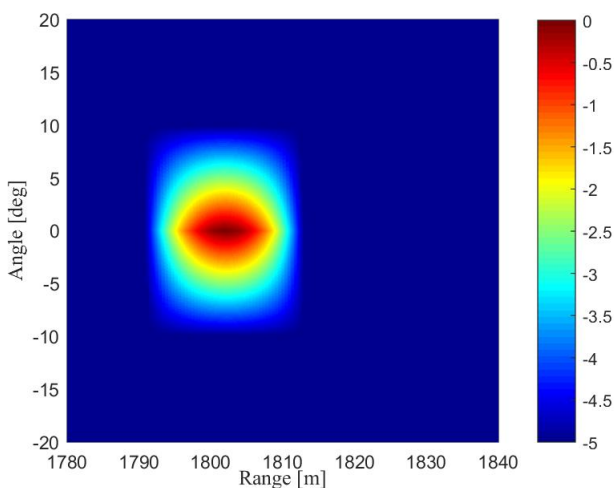


Fig. 9. The interference is suppressed by the proposed algorithm with $ISR = 10dB$.

processing, we quantitatively compare pulse compression results before and after interference mitigation, as illustrated in Fig. 4, Fig. 7, and Fig. 10.

Fig. 2 and Fig. 3 depict the power spectra of the target and interference at $ISR = -10dB$. In Fig. 2, the interference exerts minimal influence on the target, as the target signal dominates the power spectrum. Post-suppression (Fig. 3), the spectra remain virtually unchanged, demonstrating negligible distortion under low- ISR conditions.

Fig. 4 compares pulse compression results before and after suppression at $ISR = -10dB$. Before suppression, the target and interference exhibit positional offsets of approximately 9m and 80m, respectively. Post-suppression, however, the target incurs a residual offset of 1 ~ 3m due to discrepancies between the reconstructed and true interference reflection coefficients.

Fig. 5 and Fig. 6 depict the power spectra of the target and interference at $ISR = 0dB$. In Fig. 5, severe spectral overlap between the interference and target results in significant signal distortion, rendering separation infeasible. Following suppression (Fig. 6), the spectral overlap is effectively resolved, isolating the distinct power spectrum of the target. This outcome validates the efficacy of the proposed interference mitigation approach under moderate ISR conditions.

Fig. 7 illustrates a comparable scenario: pre-suppression, the target and interference exhibit overlapping positions (Fig. 5), generating ambiguous peaks in the pulse compression output. Owing to the equal power levels of the target and interference, the post-suppression residual target offset increases to 4 ~ 6m (compared to 1 ~ 3m in Fig. 4). This underscores the heightened difficulty of separating co-located signals under high ISR conditions.

Fig. 8 and Fig 9 depict the power spectra of the target and interference at $ISR = 10dB$. As illustrated in Fig. 8, the target signal is entirely obscured by the interference, leaving only the interference-dominated power spectrum discernible. Following suppression (Fig. 9), the mainlobe interference is substantially mitigated, enabling complete recovery of the target signal from the previously masked spectral profile.

Analogous to Fig. 4, the target and interference in Fig.

Fig. 2, Fig. 5, and Fig. 8. Post-suppression power spectra are correspondingly presented in Fig. 3, Fig. 6, and Fig. 9. To evaluate systematic offsets induced by suppression

10 exhibit pre-suppression positional offsets of approximately 40m and 50m, respectively. However, owing to the interference's significantly higher power compared to the target, post-suppression residual offsets increase to $7 \sim 10$ m. This result highlights the inherent challenges of signal separation in high-ISR scenarios.

The proposed close-range mainlobe interference suppression algorithm for FDA radar is rigorously validated through numerical simulations under varying ISR:

Low ISR: The interference exerts minimal influence on the target, with the target power spectrum dominating the profile. Post-suppression, the spectral characteristics remain virtually unchanged, yielding a residual target offset of $1 \sim 3$ m.

Medium ISR: Severe spectral overlap between the target and interference obscures signal separation. While suppression effectively mitigates interference, the residual offset increases to $4 \sim 6$ m, reflecting heightened complexity in resolving co-located signals.

High ISR: The interference fully masks the target signal. Despite this, the algorithm successfully recovers the target spectrum, albeit with residual offsets escalating to $7 \sim 10$ m due to the interference's dominant power.

V. CONCLUSION

In this paper, we propose a novel two-stage framework for suppressing close-range mainlobe interference in FDA radar systems, comprising interference signal reconstruction and adaptive cancellation. Through rigorous theoretical analysis and numerical simulations, we demonstrate that FDA radar exploits range-angle-decoupled DOFs—enabled by its frequency offset array architecture—to distinguish and suppress mainlobe interference signals within $1 \sim 3$ range resolution cells of the target. These results establish the capability of FDA radar to mitigate interference without relying on MIMO waveform diversity, thereby addressing a critical limitation of conventional PA and MIMO radar approaches.

Future work will expand this framework to suppress heterogeneous interference types (e.g., coherent jamming, multipath clutter) in FDA radar systems. Such advancements will advance the applicability of technology in contested electromagnetic environments, including electronic warfare and cognitive radar scenarios requiring dynamic interference resilience.

REFERENCES

- [1] W. C. Barott and B. Himed, "Time-Modulated Array Pattern for Sidelobe Blanking in Spectrometry and Radar", *IEEE Antennas and Wireless Propagation Letters*, vol. 13, pp. 1015-1018, 2014.
- [2] D. A. Shnidman and N. R. Shnidman, "Sidelobe Blanking with Expanded Models", *IEEE Transactions on Aerospace and Electronic Systems*, vol. 47, no. 2, pp. 790-805, 2011.
- [3] A. Cetronio, M. D'Urso, A. Farina, C. Lanzieri, L. Timmoneri and M. Teglia, "Phased array systems and technologies in SELEX-Sistemi Integrati: State of art and new challenges", *IEEE International Symposium on Phased Array Systems and Technology*, Waltham, MA, pp. 44-49, 2010.
- [4] Guo, R., Jiang, T., Wang, Q., Liang, R., et al. "An Improved Low-Complexity Echo Suppression Algorithm Based on the Acoustic Coloration Effect", *IAENG International Journal of Computer Science*, vol.49, no. 3, pp 637-643, 2022.
- [5] Mahyastuty, Veronica Windha, et al. "Adaptive Successive Interference Cancellation using Deep Learning for High Altitude Platform Station in Various K-Rician Channel", *IAENG International Journal of Computer Science*, vol.49, no. 2, pp 495-500, 2022.
- [6] S. Zhang, Y. Zhou, L. Zhang, Q. Zhang and L. Du, "Target Detection for Multistatic Radar in the Presence of Deception Jamming", *IEEE Sensors Journal*, vol.1, no. 1, pp 99, 2021.
- [7] W.-Q. Wang, H. C. So, A. Farina, "An overview on time/frequency modulated array processing", *IEEE Journal of Selected Topics in Signal Processing*, vol. 11, no. 2, pp. 228-246, 2017.
- [8] J. W. Xu, G. S. Liao, S. Q. Zhu, H. C. So, "Deceptive jamming suppression with frequency diverse MIMO radar", *Signal Processing*, vol. 113, no. 1, pp. 9-17, 2015.
- [9] P. F. Sannarino, C. J. Baker and H. D. Griffiths, "Frequency Diverse MIMO Techniques for Radar", *IEEE Transactions on Aerospace and Electronic Systems*, vol. 49, no. 1, pp. 201-222, 2013.
- [10] L. Lan, J. Xu, G. Liao, Y. Zhang, F. Fioranelli and H. C. So, "Suppression of Mainbeam Deceptive Jammer With FDA-MIMO Radar", *IEEE Transactions on Vehicular Technology*, vol. 69, no. 10, pp. 11584-11598, 2020.
- [11] X. Yang, Z. Zhang, T. Zeng, T. Long and T. K. Sarkar, "Mainlobe Interference Suppression Based on Eigen-Projection Processing and Covariance Matrix Reconstruction", *IEEE Antennas and Wireless Propagation Letters*, vol. 13, pp. 1369-1372, 2014.

Yisheng Yan received his M.S. and Ph.D. degrees from information and communication engineering from the School of Information and Communication Engineering (SICE), University of Electronic Science and Technology of China (UESTC), Chengdu, China, in 2014 and 2021, respectively. He is currently an engineer with Sichuan Institute of Aerospace Electronic Equipment. His research interests include radar technology, frequency diverse array signal processing, target detection.